

A Man-in-the-Middle Attack against Object Detection Systems

Han Wu, Sareh Rowlands, and Johan Wahlstrom*

Abstract—Thanks to the increasing power of CPUs and GPUs in embedded systems, deep-learning-enabled object detection systems have become pervasive in a multitude of robotic applications. While deep learning models are vulnerable to several well-known adversarial attacks, the applicability of these attacks is severely limited by strict assumptions on, for example, access to the detection system. Inspired by Man-in-the-Middle attacks in cryptography, we propose a novel hardware attack on object detection systems that overcomes these limitations. Experiments prove that it is possible to generate an efficient Universal Adversarial Perturbation (UAP) within one minute and then use the perturbation to attack a detection system via the Man-in-the-Middle attack. These findings raise serious concerns for applications of deep learning models in safety-critical systems, such as autonomous driving. Demo Video: <https://youtu.be/OvIpe-R3ZS8>.

I. INTRODUCTION

Advances in deep neural networks have made it possible to design intelligent robots that possess a more comprehensive perception of the environment than traditional robots. However, the shift to intelligent robots has been accompanied by increasing risks of adversarial attacks, particularly in safety-critical applications. It is now eight years since the first adversarial attack against neural networks, in which Goodfellow et al. fooled an image classification model by adding a small perturbation to the input image [1]. Even though the perturbation was unperceivable by humans, it still led the deep learning model to erroneous classification results. The attack was later extended from classification models to detection models and applied in an attack on an autonomous car [2].

Adversarial attacks described in the literature fall into two categories: digital attacks and physical attacks. Digital attacks apply the perturbation directly to the digital input image, whereas physical attacks print the perturbation on physical objects such as a poster [3] or a T-shirt [4]. Both digital attacks and physical attacks have their limitations. Digital perturbation requires access to the detection system so that the perturbation can be applied internally. However, in real-world scenarios, it is far from trivial to hack into a self-driving car to apply the attack. Physical attacks, on the other hand, are very sensitive to position and angle variations. For example, experiments in [2] demonstrated that an autonomous vehicle only misclassified traffic signs placed within a distance of 0.5m from the camera and viewed from specific angles. In addition, these attacks are rather inflexible. Once the adversarial object has been printed, it can only

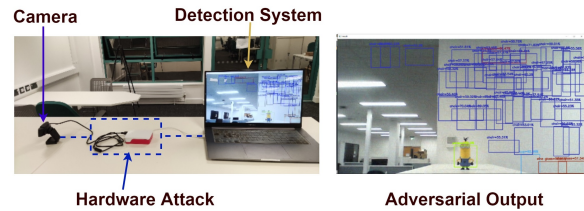
Han Wu, Sareh Rowlands, and Johan Wahlstrom are with the University of Exeter, Stocker Rd, Exeter EX4 4PY, the UK (hw630@exeter.ac.uk; s.rowlands@exeter.ac.uk; j.wahlstrom@exeter.ac.uk).



(a) Man-in-the-Middle Attack in Network Security



(b) Man-in-the-Middle Attack in Deep Learning



(c) Demo of the Hardware Attack

Fig. 1: Overview of the Man-in-the-Middle attack.

be changed through reprinting. The trial-and-error process where we search for a successful attack object may both take a long time and require massive amounts of printing.

This paper introduces a new hardware attack, inspired by Man-in-the-Middle Attacks in network security, where the attacker eavesdrops and manipulates the data transferred between a user and a server (see Fig. 1). The main contributions are as follows¹.

- 1) We propose a new hardware attack, called Man-in-the-Middle attack, that is both flexible and easy to deploy.
- 2) By using learning rate decay in the generation of the perturbation, the attack is able to generate more bounding boxes than competing attack methods that do not utilize learning rate decay.
- 3) Three new evaluation metrics are proposed. As opposed to competing evaluation metrics, these metrics do not make a binary decision for each bounding box, but are instead linear in the confidence value and probability vector.

¹The source code is available on Github: <https://github.com/wuhanstudio/adversarial-camera>

II. PRELIMINARIES

This section introduces the most widely-deployed object detection models and existing adversarial attacks against these models.

A. Object Detection Models

The object detection task is to locate the position and classify the category of each object in an image. Thus, there are two separate problems that need to be solved: localization and classification. Depending on whether these two problems are solved simultaneously or separately, we can divide existing object detection models into two categories: one-stage and two-stage methods (see Fig. 2). It is also possible to describe one-stage methods as regression or classification-based methods and two-stage methods as region proposal-based methods [5].

One-stage methods ensure computational efficiency by outputting locations and categories simultaneously. The two most widely deployed one-stage models are YOLO [6] and SSD [7]. Both YOLO and SSD can achieve real-time performance on CPUs without GPUs, which is an advantage for embedded systems. Two-stage methods consist of two steps: first, they generate a series of region proposals, and second, they classify each proposal into a specific category. Faster RCNN [8] and Mask RCNN [9] are the two most well-known two-stage methods. In addition, Mask RCNN can also solve the image segmentation task of assigning labels to each pixel instead of just outputting bounding boxes.

For robotic applications, one-stage methods are the most popular since they are faster and still provide acceptable accuracy in most situations. Two-stage methods are generally more accurate but also more computationally expensive. The use of GPUs puts larger demands on cooling system efficiency and battery capacity, which may lead to bottlenecks in real-time robotic applications. Nevertheless, both one-stage and two-stage models are vulnerable to adversarial attacks. In this study, we intend to investigate how these attacks affect real-time robotic applications. As a result, we focus on the more energy efficient one-stage models, YOLO and SSD.

B. Adversarial Attacks on Object Detection Models

The first adversarial attack against classification models, published in 2014, used the Fast Gradient Sign Method

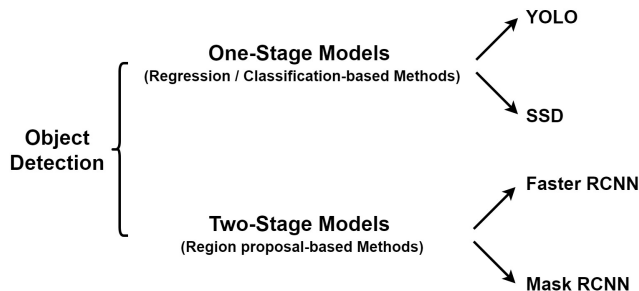


Fig. 2: The most widely used object detection models.

(FGSM) [1]. This method uses gradients to generate image-specific perturbations. If the input image changes, the perturbation needs to be regenerated. For real-world robotic applications, it is more practical to use image-agnostic perturbations, known as Universal Adversarial Perturbations (UAPs). This type of attack was first presented in [10], which fooled classification models on most images in a dataset using a single perturbation. Later, adversarial attacks were extended from image classification to image segmentation [11] and detection models [12].

In addition to image-specific and image-agnostic methods, it is also possible to classify adversarial attacks into data-driven and data-independent approaches. Data-driven approaches require access to the input image, while data-independent methods only need access to the parameters and architecture of the target model. Generally, data-driven approaches achieve a higher fooling rate as they have more information at their disposal. Data-driven methods include gradient-based methods, methods using Generative Adversarial Networks (GANs), and optimization-based methods. Gradient-based methods use gradients to maximize the adversarial loss. The adversarial loss functions can be designed in multiple different ways [13], [14], [15]. It is also possible to train GANs to generate adversarial examples [16], [17]. Finally, the attack problem can be transformed into the optimization problem of minimizing the perturbation while maximizing the training loss [18], [19].

By adding extra constraints to data-driven methods these can also be used to generate physical perturbations [3]. For example, it is possible to add the Sub-sampled Non-Printability Score (SNPS) constraint to the loss function. The Non-Printability Score (NPS) measures the error between a printed pixel and its digital counterpart. Additional constraints can be used to generate physical perturbations that preserve the adversarial effect if printed out on a poster. Methods for generating and applying perturbations are summarized in Fig. 3.

In the next section, we devise our gradient-based data-driven method that generates image-agnostic UAPs and then applies the perturbation via the Man-in-the-Middle attack.

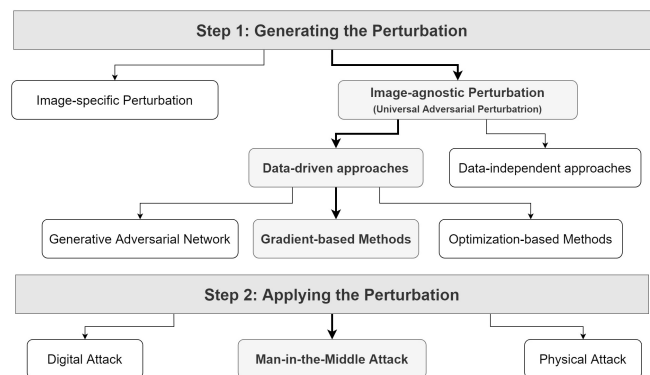


Fig. 3: Popular methods for generating and applying adversarial perturbations.

III. MAN-IN-THE-MIDDLE ATTACK

This section introduces a gradient-based method, named the PCB attack, to generate the Universal Adversarial Perturbation (UAP). We then apply the perturbation via a novel hardware attack inspired by the Man-in-the-Middle Attack in cryptography. We name our attack the PCB attack because we handle the output of probability vector (P), confidence value (C), and bounding boxes separately (B). Besides, the acronym of PCB is fitting for a hardware attack, since this acronym is also used for Printed Circuit Boards (PCB).

A. Problem Formulation

As described in Section II, existing object detection models consist of one-stage models (YOLO, SSD) and two-stage models (Faster-RCNN, Mask-RCNN). Though different models have different structures, they share similar inputs and outputs. We use the following mathematical notation to describe these inputs and outputs.

- x : The original clean input image.
- δ : The adversarial perturbation.
- x' : The adversarial input image $x' = x + \delta$.
- K : The total number of candidate classes.
- N : The total number of candidate bounding boxes.
- $\mathcal{O}(x)$: The output of N candidate bounding boxes from the model given the input image x .
- $o_i(x)$: The i_{th} output in $\mathcal{O}(x) = \{o_1, o_2, o_3, \dots, o_N\}$, where $o_i = (b_i, c_i, p_i)$. $1 \leq i \leq N$.
- b_i : The location and dimension of the i_{th} candidate box. $b_i = (b_i^x, b_i^y, b_i^w, b_i^h)$ represents a bounding box at position (b_i^x, b_i^y) with width b_i^w and height b_i^h ,
- c_i : The confidence value (objectness) of the i_{th} candidate box that represents how probable it is that the candidate box represents an object.
- p_i : The softmax probability vector of the i_{th} candidate box. $p_i = (p_i^1, p_i^2, \dots, p_i^K)$ for K classes and $\sum p_i = 1$.

Putting things together: Given an input image x , the object detection model outputs N candidate bounding boxes $\mathcal{O}(x) = \{o_1, o_2, o_3, \dots, o_N\}$. Each candidate box $o_i = (b_i, c_i, p_i)$ contains $b_i = (b_i^x, b_i^y, b_i^w, b_i^h)$ that represents the location and dimension of the box, the confidence value $c_i \in [0, 1]$ that represents how probable it is that the candidate box represents an object, and the softmax probability vector, $p_i = (p_i^1, p_i^2, \dots, p_i^K)$ for K classes. The raw outputs from the detection model $\mathcal{O}(x)$ may contain several thousand candidate bounding boxes. We then use the Non-maximum Suppression (NMS) method [20] to filter out bounding boxes with low confidence values, and high Intersection over Union (IoU) to generate final detection results.

An adversarial example x' aims to fool the detection model so that it outputs candidate boxes $\mathcal{O}(x') \neq \mathcal{O}(x)$. For example, the adversarial output $\mathcal{O}(x')$ may detect more false positive objects after the NMS. Next, we will describe how to generate the perturbation δ .

B. Generating the perturbation (PCB Attack)

Gradient-based methods use similar approaches to generate image-specific and image-agnostic perturbations. Given

an input image, we iterate over a single image to produce an image-specific perturbation. Given the entire dataset, we then iterate over multiple images to generate the UAP. Thus, we first introduce how we generate image-specific perturbations and then extend the attack to its image-agnostic counterpart.

1) **Image-specific PCB Attack**: The intuition behind gradient-based methods is straightforward. During the training process, we minimize the training loss

$$\min_{\mathcal{W}} \mathcal{L}_{train} = f(\mathcal{W}; x, \mathcal{O}) \quad (1)$$

by updating the model weights. Note that the training loss is a function of the input x , the model weights \mathcal{W} , and the ground truth \mathcal{O} . However, our objective is to fool the detection model to make inaccurate predictions. Therefore, during the attack, we maximize the adversarial loss

$$\max_x \mathcal{L}_{adv} = f(x; \mathcal{O}^*, \mathcal{W}) \quad (2)$$

by updating the input x and using the desired adversarial outputs \mathcal{O}^* . Different gradient-based methods use different adversarial loss functions \mathcal{L}_{adv} and construct desired adversarial outputs \mathcal{O}^* differently. In our attack, we separate the Probability vector and Confidence value (PC) with Bounding boxes (B) and investigate the two adversarial loss functions

$$\mathcal{L}_{PC}(x) = \sum \sigma(c_i) * \sigma(p_i) \quad (3)$$

and

$$\mathcal{L}_{PCB}(x) = \frac{\sum (\sigma(c_i) * \sigma(p_i))}{\sum [\sigma(w_i) * \sigma(h_i)]^2}. \quad (4)$$

Using $\mathcal{L}_{PCB}(x)$ will give smaller bounding boxes, while $\mathcal{L}_{PC}(x)$ gives larger bounding boxes. By maximizing the adversarial loss, we generate large amounts of incorrect bounding boxes (fabrication attack). By minimizing the loss, we remove bounding boxes (vanishing attack).

The optimization of (2) is performed by first zero-initializing the perturbation δ , and then using Projected Gradient Descent (PGD) [21] with learning rate decay so that

$$\delta_{t+1} = \text{proj}_p(\delta_t + \alpha \text{sign}(\frac{\partial \mathcal{L}_{adv}(x'_t; \mathcal{O}^*)}{\partial x'_t})). \quad (5)$$

The image-specific PCB attack is summarized in Algorithm 1, where $\text{proj}_{\infty}(\delta, \epsilon)$ is the projection function $\min(\delta, \epsilon)$ and $\text{clip}(-1, 1)$ is the unit clip function.

2) **Image-agnostic PCB Attack**: We can extend the method to an image-agnostic attack by iterating over a collection of images X_s , representing all available images to the attacker. X_s can be thought of as the training set or a video clip from the target scene. In each iteration, we iterate the perturbation δ over X_s . The learning rate α should be relatively small compared to the image-specific PCB attack. We summarize the image-agnostic PCB attack in the algorithm 2 and discuss how we choose hyper-parameters in the next section.

Algorithm 1 Image-specific PCB Attack

Input: The target model, the input image x .
 Parameters: The learning rate α , learning rate decay k , number of iterations n , and strength of the attack ϵ .
 Output: Image-specific perturbation δ
 Initialize $\delta \leftarrow 0$
for $i = 1 : n$ **do**
 $x' = x + \delta$
 $\nabla = \frac{\partial L_{adv}(x'; O^*)}{\partial x'}$
 $\delta \leftarrow \delta + \alpha * \text{sign}(\nabla)$
 $\delta \leftarrow \text{clip}(-1, 1)$
 $\delta \leftarrow \text{proj}_{\infty}(\delta, \epsilon)$
 $\alpha = \alpha * k$
end for

Algorithm 2 Image-agnostic PCB Attack (UAP)

Input: The target model, the sample images X_S .
 Parameters: The learning rate α , learning rate decay k , number of iterations n , and strength of the attack ϵ .
 Output: Image-specific perturbation δ
 Initialize $\delta \leftarrow 0$
for $i = 1 : n$ **do**
 for each image $x \in X_S$ **do**
 $x' = x + \delta$
 $\nabla = \frac{\partial L_{adv}(x')}{\partial x'}$
 $\delta \leftarrow \delta + \alpha * \text{sign}(\nabla)$
 $\delta \leftarrow \text{clip}(-1, 1)$
 $\delta \leftarrow \text{proj}_p(\delta, \epsilon)$
 end for
 $\alpha = \alpha * k$
end for

C. Applying the perturbation (Man-in-the-Middle Attack)

In Section I, it was mentioned that the biggest hurdle for the digital attack is not having access to the internal system. In digital attacks, the perturbation is of the same size as the model input (YOLO 416x416) since it is generated using the gradient of the model input over the adversarial loss. However, in real-world applications, the resized image is a temporary variable in the middle of the detection system. Thus, to conduct a digital attack, we need to hack into the operating system and inject malicious code into the embedded system, which is not trivial.

To solve this problem, we devise the Man-in-the-Middle hardware attack. Notice that the camera that captures the image is exposed directly to the outside world without any protection. If we eavesdrop and manipulate the image data before it has reached the detection system, we can apply the perturbation without access to the operating system.

1) **Hardware Implementation:** To perform the Man-in-the-Middle attack, we need hardware that reads raw images from the USB camera and injects the perturbation. In addition, we also need to simulate a virtual camera to the detection system. In this way, the operating system is not aware of that the camera is under attack since it still

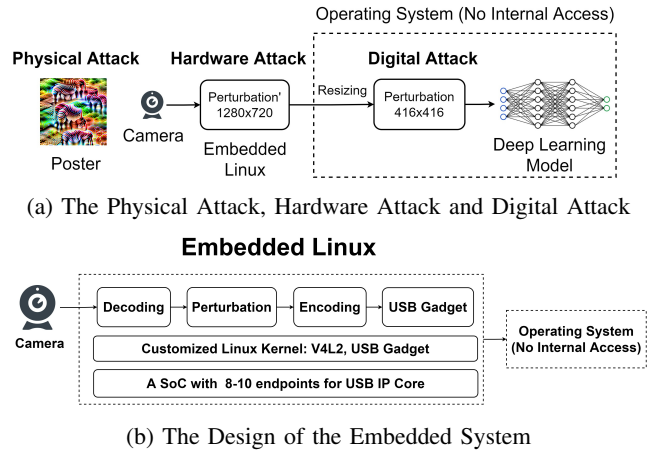


Fig. 4: The System Architecture.

detects a USB camera device. There is a lot of hardware capable of reading images from a USB camera, but it is more challenging to simulate a virtual USB camera. We find that Raspberry Pi Zero, Raspberry Pi 4, and IMX6UL satisfies the requirement. Moreover, a proper Linux kernel that supports the V4L2 driver, the USB gadget framework, and configs is required to drive the hardware. The overall architecture of the system design is illustrated in Fig. 4.

2) **Resizing the perturbation:** When performing the attack on the hardware rather than on the object detection system, the perturbation will be applied before pre-processing (resizing). For example, the input shape of YOLO and the perturbation is 416x416. However, the image shape of a typical USB camera might be 1280x720. To understand the implications of this, we will use \mathcal{R} to denote the resize function that downscales an image ($1280 \times 720 \rightarrow 416 \times 416$), and \mathcal{R}^{-1} to denote the one that upscales an image ($416 \times 416 \rightarrow 1280 \times 720$). For image resizing functions that use bilinear interpolation it then holds that

$$\mathcal{R}(x'_o) = \mathcal{R}(x_o + \mathcal{R}^{-1}(\delta)) = \mathcal{R}(x_o) + \mathcal{R}\mathcal{R}^{-1}(\delta) \quad (6)$$

where x'_o and x_o are the original 1280x720 images with and without applied perturbations, respectively. However, after resizing, the adversarial input constructed by the Man-in-the-Middle attack is different from a valid adversarial input $\mathcal{R}(x_o) + \delta$, that is,

$$\mathcal{R}(x_o) + \mathcal{R}\mathcal{R}^{-1}(\delta) \neq \mathcal{R}(x_o) + \delta. \quad (7)$$

Our experimental results demonstrate that the adversarial effect is preserved even though the resize function is not invertible.

IV. EXPERIMENTAL EVALUATION

This section explains why the Mean Accuracy Precision (mAP) is not suitable for adversarial attacks evaluation. Following this, we compare different initialization methods, adversarial loss functions, and investigate the efficiency of using learning rate decay.



(a) mAP cannot distinguish between fabrication and vanishing attacks.



(b) mAP does not consider confidence values.

Fig. 5: Illustration of the limitations of mAP.

A. Evaluation Metrics

The mAP [22] is typically used to both to measure the accuracy of object detection models and to evaluate the strength of adversarial attacks. However, it can be noticed that the mAP cannot distinguish between different attacks. For example, both the fabrication and vanishing attacks result in an $mAP \approx 0$, even though they serve different attacking purposes (see Fig. 5a). Similarly, while an attacker will prefer a stronger attack (Dog 99%) over a weaker attack (Dog 60%), mAP does not reflect the strength of an attack (see Fig. 5b). In addition, note that the overall detection error

$$\begin{aligned} \mathcal{O}(x') - \mathcal{O}_{true} &= [\mathcal{O}(x') - \mathcal{O}(x)] + [\mathcal{O}(x) - \mathcal{O}_{true}] \\ &= \varepsilon_{\text{attack}} + \varepsilon_{\text{model}}, \end{aligned} \quad (8)$$

where \mathcal{O}_{true} is the ground truth model output, includes the attack error $\varepsilon_{\text{attack}}$ and the model error $\varepsilon_{\text{model}}$. The mAP measures the overall error by comparing the adversarial outputs with the ground truth, but we are only interested in the attack error $\mathcal{O}(x') - \mathcal{O}(x)$. Therefore, we devise three new evaluation metrics.

- 1) Mean Confidence Variation: The average increase or decrease of the confidence value of all the bounding boxes at each iteration step t . This metric reflects the strength of the attack on the confidence value and is expressed as $\frac{1}{N} \sum_{i=1}^N (c_{t,i} - c_{t-1,i})$.
- 2) Number of Boxes: The total number of bounding boxes after the NMS. This metric shows how many objects are detected at each step of the attack $|\text{NMS}(\mathcal{O}(x))|$.
- 3) Relative Box Variation: After each iteration, the position of false positive bounding boxes fluctuates. This metric measures the percentage of consistent bounding boxes (bounding boxes that have the same position as in the previous step) at the current step and can be expressed as $\frac{|\text{NMS}(\mathcal{O}(x_t))| + |\text{NMS}(\mathcal{O}(x_{t-1}))| - |\text{NMS}(\mathcal{O}(x'_t), \mathcal{O}(x'_{t-1}))|}{|\text{NMS}(\mathcal{O}(x_t))|}$.

The adversarial loss determines the type of attack (fabrication or vanishing), while the iteration process determines

the strength of the attack. Thus, we use our new evaluation metrics to study the iteration process to achieve more efficient attacks against a one-stage detection model (YOLO). The experiments used the VOC2012 dataset [23].

B. Initialization Method

The state-of-the-art TOG attack uses uniform initialization [13]. However, several other attacks have used zero initialization [11], [14], [15], [21]. Gradient-based attacks hinge on gradients to iterate from the original image to an adversarial input. Intuitively, uniform initialization may counteract the gradient at the first step. We conduct 5 runs of the PCB attack using uniform initialization, and compare the results with zero-initialization (see Fig. 6).

The third evaluation metric, relative box variation, converges to 1, indicating that all false positive bounding boxes are stable. Different initialization methods result in similar convergence speeds. The first and second evaluation metrics, mean confidence variation and number of boxes, measure the strength of the attack. Only one in five runs of uniform initialization results in a more efficient attack than zero initialization, which confirms our hypothesis that uniform initialization counteracts the initial gradients.

C. Learning Rate Decay

To achieve an efficient attack, we need to avoid gradient counteraction which can make the attack vary a lot over iterations. Thus, the PCB attack introduces the learning rate decay k to make the attack more stable over different iterations.

The original PGD attack does not use learning rate decay ($k = 1.00$). As a result, the iteration process is rather unstable (the black line in Fig. 7), making it difficult to achieve an efficient attack. This problem has not been studied in prior research, which has only used mAP as the evaluation metric. Even though the iteration process may be unstable, the value of mAP will still be low and stable. For example, at each step, we generate different false positive bounding boxes at various positions, but none of them matches the ground truth ($mAP = 0$). As a result, even though the location of bounding boxes varies a lot from one iteration to the next, the mAP remains at 0.

Using our new evaluation metrics, we can see the complete iteration process (see Fig. 7). As the learning rate decay k decreases from 0.99 to 0.90, more iterations are required before the two evaluation metrics, the mean confidence variation and the number of boxes, converges. However, they both converge at higher values when k decreases, indicating that the attack is more efficient. In other words, learning rate decay helps to achieve efficient adversarial attacks.

D. Adversarial Loss Function

Finally, we compare the three adversarial loss functions of the fabrication attack. Our objective is not to find the best loss function but to highlight the advantages and disadvantages of different methods using our evaluation metrics.

In Fig. 8, the Relative Box Variation of all the three methods converges to 1, indicating that locations of almost

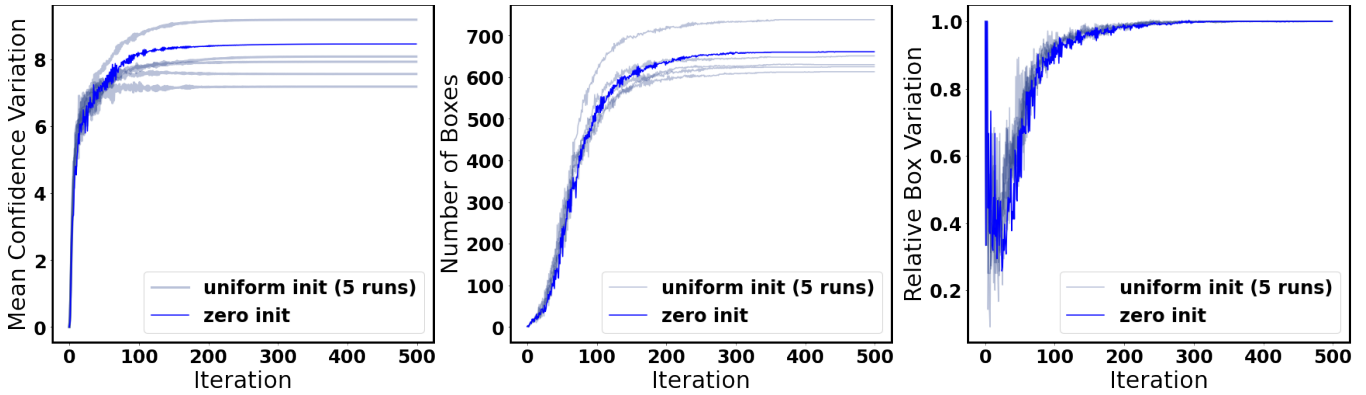


Fig. 6: The PCB fabrication attack using different initialization methods.

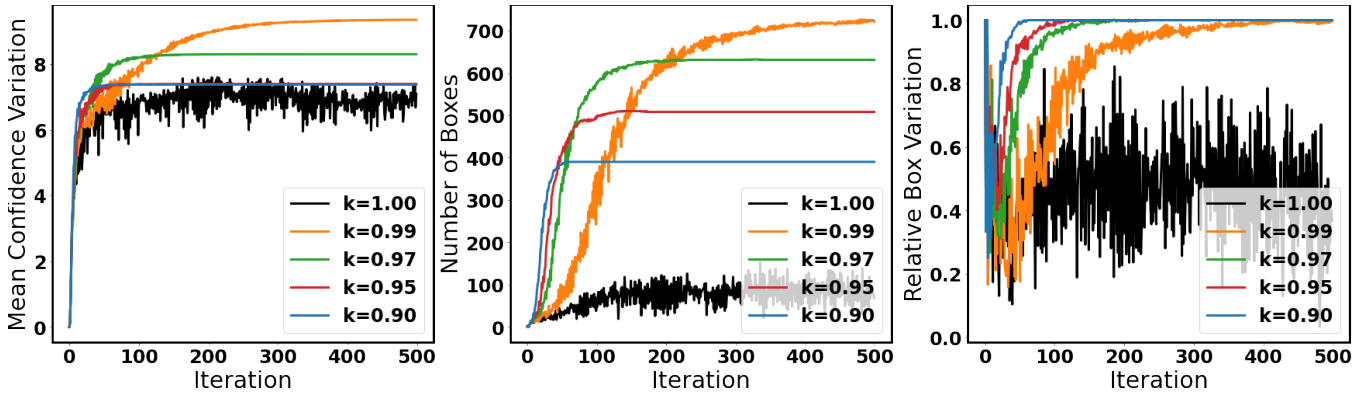


Fig. 7: The PCB fabrication attack with different learning rate decays.

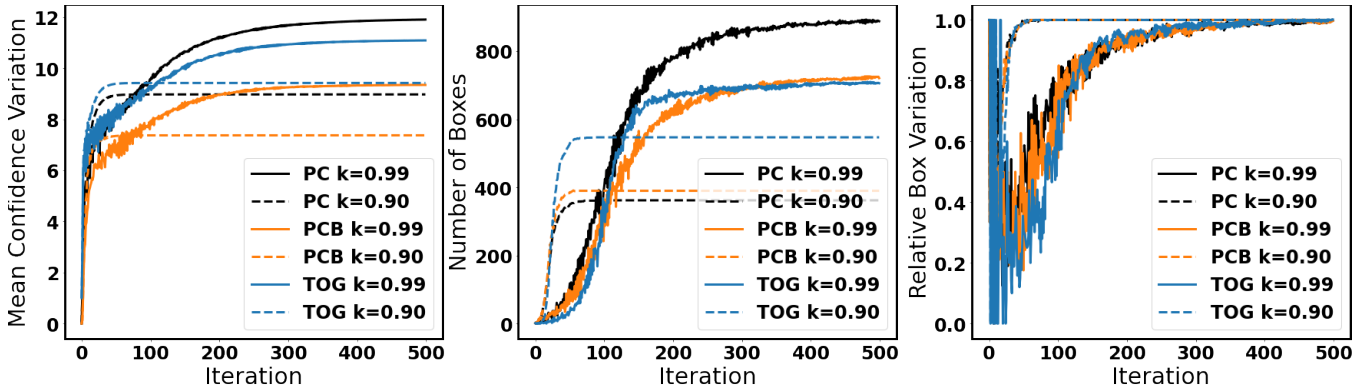


Fig. 8: Different adversarial loss functions of the fabrication attack.

all the bounding boxes are stable in the final iterations. Though the PC attack generates the most bounding boxes and achieves the highest Mean Confidence Variation when $k = 0.99$, it requires a larger number of iterations to reach the plateau. If the number of available sample images X_s is large, the PC attack requires more computational resources and time. On the other hand, the TOG and the PCB attack prevail over the PC attack when $k = 0.90$, and they converge faster. Therefore, we cannot conclude that a single method prevails over the others. Instead, the newly proposed evaluation metrics are good references for decision-making.

V. CONCLUSIONS

This paper exposes a previously unknown vulnerability of deep learning object detection systems that have serious implications for a range of safety-critical applications. As opposed to competing attack frameworks, the proposed attack does not assume access to the object detection system, but instead relies on perturbations injected on the hardware level. The efficiency of the attack was demonstrated in experiments using the VOC2012 dataset and the YOLO detection model. Future work may focus on extending the attack to tasks other than object detection or to other sensors, such as Lidar.

REFERENCES

- [1] I. Goodfellow, J. Shlens, and C. Szegedy, "Explaining and harnessing adversarial examples," in *International Conference on Learning Representations (ICLR)*, 2015.
- [2] J. Lu, H. Sibai, E. Fabry, and D. A. Forsyth, "No need to worry about adversarial examples in object detection in autonomous vehicles," in *Proceedings of the IEEE Conference on Computer Vision and Pattern Recognition (CVPR)*, 2017.
- [3] M. Lee and Z. Kolter, "On physical adversarial patches for object detection," *arXiv preprint arXiv:1906.11897*, 2019.
- [4] K. Xu, G. Zhang, S. Liu, Q. Fan, M. Sun, H. Chen, P.-Y. Chen, Y. Wang, and X. Lin, "Adversarial t-shirt! evading person detectors in a physical world," in *European Conference on Computer Vision (ECCV)*, 2020, pp. 665–681.
- [5] Z.-Q. Zhao, P. Zheng, S.-T. Xu, and X. Wu, "Object detection with deep learning: A review," *IEEE Transactions on Neural Networks and Learning Systems*, vol. 30, no. 11, pp. 3212–3232, 2019.
- [6] J. Redmon, S. Divvala, R. Girshick, and A. Farhadi, "You only look once: Unified, real-time object detection," in *Proceedings of the IEEE conference on computer vision and pattern recognition*, 2016, pp. 779–788.
- [7] W. Liu, D. Anguelov, D. Erhan, C. Szegedy, S. Reed, C.-Y. Fu, and A. C. Berg, "Ssd: Single shot multibox detector," in *European conference on computer vision*. Springer, 2016, pp. 21–37.
- [8] S. Ren, K. He, R. Girshick, and J. Sun, "Faster r-cnn: Towards real-time object detection with region proposal networks," *Advances in neural information processing systems*, vol. 28, 2015.
- [9] K. He, G. Gkioxari, P. Dollár, and R. Girshick, "Mask r-cnn," in *Proceedings of the IEEE international conference on computer vision*, 2017, pp. 2961–2969.
- [10] S.-M. Moosavi-Dezfooli, A. Fawzi, O. Fawzi, and P. Frossard, "Universal adversarial perturbations," in *Proceedings of the IEEE conference on computer vision and pattern recognition*, 2017, pp. 1765–1773.
- [11] V. Fischer, M. C. Kumar, J. H. Metzen, and T. Brox, "Adversarial examples for semantic image segmentation," *arXiv preprint arXiv:1703.01101*, 2017.
- [12] R. Gurbaxani and S. Mishra, "Traits & transferability of adversarial examples against instance segmentation & object detection," *arXiv preprint arXiv:1808.01452*, 2018.
- [13] K.-H. Chow, L. Liu, M. Loper, J. Bae, M. E. Gursoy, S. Truex, W. Wei, and Y. Wu, "Adversarial objectness gradient attacks in real-time object detection systems," in *2020 Second IEEE International Conference on Trust, Privacy and Security in Intelligent Systems and Applications (TPS-ISA)*. IEEE, 2020, pp. 263–272.
- [14] D. Li, J. Zhang, and K. Huang, "Universal adversarial perturbations against object detection," *Pattern Recognition*, vol. 110, p. 107584, 2021.
- [15] O. Mohamad Nezami, A. Chaturvedi, M. Dras, and U. Garain, "Pick-object-attack: Type-specific adversarial attack for object detection," *Comput. Vis. Image Underst.*, vol. 211, no. C, oct 2021.
- [16] A. S. Hashemi, A. Bär, S. Mozaffari, and T. Fingscheidt, "Transferable universal adversarial perturbations using generative models," *arXiv preprint arXiv:2010.14919*, 2020.
- [17] X. Wei, S. Liang, N. Chen, and X. Cao, "Transferable adversarial attacks for image and video object detection," in *Proceedings of the Twenty-Eighth International Joint Conference on Artificial Intelligence, IJCAI-19*. International Joint Conferences on Artificial Intelligence Organization, 7 2019, pp. 954–960.
- [18] N. Carlini and D. Wagner, "Towards evaluating the robustness of neural networks," in *2017 IEEE Symposium on Security and Privacy (SP)*. Ieee, 2017, pp. 39–57.
- [19] Q. Liao, X. Wang, B. Kong, S. Lyu, B. Zhu, Y. Yin, Q. Song, and X. Wu, "Transferable adversarial examples for anchor free object detection," in *2021 IEEE International Conference on Multimedia and Expo (ICME)*. IEEE, 2021, pp. 1–6.
- [20] N. Bodla, B. Singh, R. Chellappa, and L. S. Davis, "Soft-nms improving object detection with one line of code," in *Proceedings of the IEEE international conference on computer vision*, 2017, pp. 5561–5569.
- [21] A. Madry, A. Makelov, L. Schmidt, D. Tsipras, and A. Vladu, "Towards deep learning models resistant to adversarial attacks," *arXiv preprint arXiv:1706.06083*, 2017.
- [22] J. Cartucho, R. Ventura, and M. Veloso, "Robust object recognition through symbiotic deep learning in mobile robots," in *2018 IEEE/RSJ International Conference on Intelligent Robots and Systems (IROS)*, 2018, pp. 2336–2341.
- [23] M. Everingham, L. Van Gool, C. K. I. Williams, J. Winn, and A. Zisserman, "The PASCAL Visual Object Classes Challenge 2012 (VOC2012) Results," <http://www.pascal-network.org/challenges/VOC/voc2012/workshop/index.html>.